

Photocurrent measurements on graphene devices using the attoCFM II.

The model of edge-state transport is commonly accepted for interpreting many of the effects seen in Quantum Hall Effect (QHE) devices. Although compressible and incompressible electron densities have recently been observed in graphene, their role in shaping the QHE in graphene remains to be explained. Spatially inhomogeneous charge distributions owing to adsorbate-induced surface doping are expected to be particularly pronounced in graphene and could cause deviations from pure edge-state transport.

In this application note, G. Nazin and P. Sutter present spatially resolved photocurrent measurements on a graphene field-effect device in the QHE regime to study the distribution of Landau levels and its relation with macroscopic transport characteristics.

The experiments were carried out using an attocube attoCFM II optical microscope for low temperatures and high magnetic fields. Fig. 1a shows an optical image of the measured device. Fig. 1b shows a schematic sketch of the experiment. Photocurrent maps were obtained by scanning a focused laser across the graphene channel, and recording the two-terminal (source-drain) photocurrent signal as a function of beam position.

The net photocurrent is determined by hot carriers transported to the periphery of the graphene channel, where QHE edge states provide efficient pathways for their extraction to the contacts. To further analyze these periodically recurring photocurrent distributions, we consider the photocurrent as a function of gate voltage along a line across the graphene channel. In a perpendicular magnetic field, the energy-level spectrum of Dirac fermions in graphene comprises n - and p -type Landau levels, as well as a degenerate level $n=0$ at the neutrality point (Fig. 2a). In the photocurrent section of Fig. 2b, every Landau level except $n=0$ is associated with a distinct 'butterfly' pattern comprising four lobes of alternating polarity. The sign of the photocurrent response changes abruptly on crossing the channel centerline, and on either side alternates with varying VG. A model based on hot-carrier transport explains this characteristic photocurrent pattern (Fig. 2c,d). Photocurrent maps used to image Landau levels within the entire graphene channel show that the energies of Landau levels are higher in the centre than at the edges (Fig. 3). This type of band bending has been observed in all tested devices, and similar band bending is probably present to some degree in all graphene devices used in conventional transport experiments.

In summary, photocurrent measurements performed on graphene field-effect devices provided insight into carrier transport and the distribution of energy levels in the QHE regime. The exceptional stability and the ease of use of the attoCFM II microscope greatly facilitated these measurements and allowed for measuring working devices in magnetic fields from -9 to $+9T$.

Reprinted with permission from G. Nazin, Y. Zhang, L. Zhang, E. Sutter, P. Sutter, *Nature Physics* 6, 870–874 (2010). © 2010, Nature Physics.

Reference:

[1] G. Nazin, *Nature Physics* 6, 870–874 (2010).

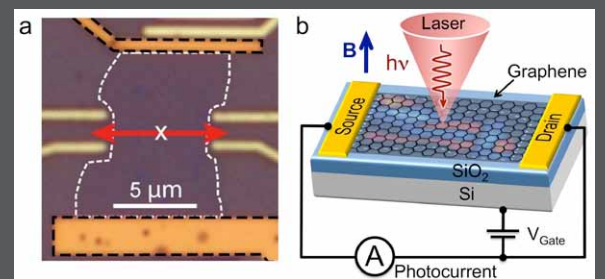


Fig. 1: Photocurrent measurements on graphene devices. (a) Optical image of the device. The dashed outlines mark the channel and the two connected electrodes. The four side electrodes are not in contact with the device. (b) Schematic of the photocurrent measurement.

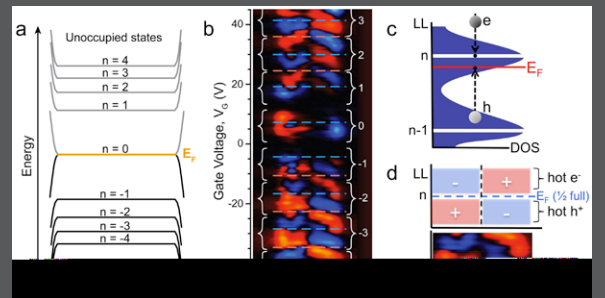


Fig. 2: (a) Landau levels (LLs) in graphene. At the edges, the magnetic field bends levels with $n>0$ ($n<0$) upward (downward); the degenerate $n=0$ level splits into two branches. (b) Measured gate voltage dependence of photocurrent across the device (along the arrow shown in Fig. 1a) extracted from 240 individual scans across the graphene channel for VG from -45 V to $+45$ V ($B=9T$). The braces indicate the VG ranges corresponding to individual Landau levels, numbered sequentially $n=0, \pm 1, \pm 2$ and so on. (c) Model of local filling factor controlling the phase space for hot-carrier relaxation to EF. Carriers relaxing to localized states in the disorder-broadened LLs dominate the photocurrent. (d) Predicted pattern of hot electron and hole transport, and comparison with experiment.

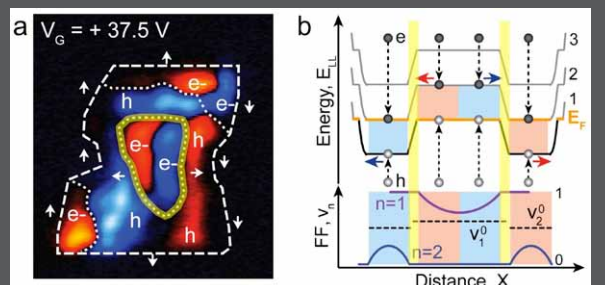


Fig. 3: Mapping Landau levels in the presence of band bending in graphene. (a) Experimental Landau level map, determined by photocurrent microscopy at $B=9T$. (b) Schematic representation of Landau levels and filling factor across the device. Yellow stripes mark the position of the incompressible boundary between $n=1$ and $n=2$ levels.